Supplemental Material: Are multiphase competition & order-by-disorder the keys to understanding $\text{Yb}_2\text{Ti}_2\text{O}_7$?

L.D.C. Jaubert,[1] Owen Benton,[1] Jeffrey G. Rau,[2] J. Oitmaa,[3]
R.R.P. Singh,[4] Nic Shannon,[1] and Michel J.P. Gingras[2, 5, 6]

[1] *Okinawa Institute of Science and Technology Graduate University, Onna-son, Okinawa 904-0395, Japan*
[2] *Department of Physics and Astronomy, University of Waterloo,*
200 University Avenue West, Waterloo, Ontario, N2L 3G1, Canada
[3] *School of Physics, The University of New South Wales, Sydney 2052, Australia*
[4] *Department of Physics, University of California, Davis, California 95616, USA*
[5] *Perimeter Institute for Theoretical Physics, 31 Caroline North, Waterloo, Ontario, N2L 2Y5, Canada*
[6] *Canadian Institute for Advanced Research, Toronto, Ontario, M5G 1Z8, Canada*

ORDER PARAMETERS AND CORRELATORS

As illustrated in Fig. 1 of the main text, three main phases are studied in this paper: the U(1) manifold, divided into ψ_2 and ψ_3 phases, and the splayed ferromagnet (SFM). Their order parameters can be found in the literature [1–5] and are repeated below for convenience.

In what follows, we adopt the convention of Ref. [6] regarding the labeling of the spins, defined by their positions relative to the centre of the tetrahedron

$$\vec{r}_0 = \left(\frac{1}{2}, \frac{1}{2}, \frac{1}{2}\right), \quad \vec{r}_1 = \left(\frac{1}{2}, -\frac{1}{2}, -\frac{1}{2}\right),$$
$$\vec{r}_2 = \left(-\frac{1}{2}, \frac{1}{2}, -\frac{1}{2}\right), \quad \vec{r}_3 = \left(-\frac{1}{2}, -\frac{1}{2}, \frac{1}{2}\right). \quad (1)$$

The spins at the four sites are denoted as $\vec{S}_{i=0,1,2,3} = (S_i^x, S_i^y, S_i^z)$ in the cubic coordinates, with $|\vec{S}_i| = 1/2$.

For the U(1) manifold, the order parameter, per tetrahedron, is a two-dimensional vector.

$$\vec{m}_{\text{U}(1)} = \begin{pmatrix} m_{\text{U}(1)}^\alpha \\ m_{\text{U}(1)}^\beta \end{pmatrix} = \begin{pmatrix} \frac{1}{2\sqrt{6}}\left(-2S_0^x + S_0^y + S_0^z - 2S_1^x - S_1^y - S_1^z + 2S_2^x + S_2^y - S_2^z + 2S_3^x - S_3^y + S_3^z\right) \\ \frac{1}{2\sqrt{2}}\left(-S_0^y + S_0^z + S_1^y - S_1^z - S_2^y - S_2^z + S_3^y + S_3^z\right) \end{pmatrix} \quad (2)$$

To differentiate between the ψ_2 and ψ_3 states within the U(1) manifold, we define the angle $\theta_{\text{U}(1)} = \arctan(m_{\text{U}(1)}^\beta / m_{\text{U}(1)}^\alpha)$; the function $\cos(6\theta_{\text{U}(1)})$ respectively equals to $+1$ and -1 for ψ_2 and ψ_3 states [1, 4, 5].

As for the splayed ferromagnetic phase, it is fully described by two three-dimensional order parameters [4]

$$\vec{m}_{\text{SFM1}} = \begin{pmatrix} m_{\text{SFM1}}^\alpha \\ m_{\text{SFM1}}^\beta \\ m_{\text{SFM1}}^\gamma \end{pmatrix} = \begin{pmatrix} \frac{1}{2}(S_0^x + S_1^x + S_2^x + S_3^x) \\ \frac{1}{2}(S_0^y + S_1^y + S_2^y + S_3^y) \\ \frac{1}{2}(S_0^z + S_1^z + S_2^z + S_3^z) \end{pmatrix}, \quad (3)$$

$$\vec{m}_{\text{SFM2}} = \begin{pmatrix} m_{\text{SFM2}}^\alpha \\ m_{\text{SFM2}}^\beta \\ m_{\text{SFM2}}^\gamma \end{pmatrix}$$
$$= \begin{pmatrix} \frac{-1}{2\sqrt{2}}(S_0^y + S_0^z - S_1^y - S_1^z - S_2^y + S_2^z + S_3^y - S_3^z) \\ \frac{-1}{2\sqrt{2}}(S_0^x + S_0^z - S_1^x + S_1^z - S_2^x - S_2^z + S_3^x - S_3^z) \\ \frac{-1}{2\sqrt{2}}(S_0^x + S_0^y - S_1^x + S_1^y + S_2^x - S_2^y - S_3^x - S_3^y) \end{pmatrix} \quad (4)$$

where $\vec{m}_{\text{SFM1}}$ is simply the global magnetization and $\vec{m}_{\text{SFM2}}$ accounts for the splayed nature of the ferromagnetism, *i.e.* the fact that the spins are not colinear. For a given SFM ground state, both $\vec{m}_{\text{SFM1}}$ and $\vec{m}_{\text{SFM2}}$ are finite.

In order to compare the growth of correlations between the two phases, we define the order-parameter correlators

$$C_{IJ} = \langle m_I m_J \rangle - \langle m_I \rangle \langle m_J \rangle \quad (5)$$

where m_I is the order parameter of phase I. For the U(1) manifold, the use of the correlators is rather straightforward. However, for the SFM phase, since both $\vec{m}_{\text{SFM1}}$ and $\vec{m}_{\text{SFM2}}$ are finite, one needs to compute the matrix of correlators

$$\begin{pmatrix} C_{\text{SFM1,SFM1}} & C_{\text{SFM1,SFM2}} \\ C_{\text{SFM2,SFM1}} & C_{\text{SFM2,SFM2}} \end{pmatrix}. \quad (6)$$

By definition, this matrix is symmetric but a priori non-diagonal. Upon diagonalization, the maximum eigenvalue is kept as correlator of the SFM phase. Please

MONTE CARLO SIMULATIONS

Fig. 1 in the main text has been obtained by classical Monte Carlo simulations of Heisenberg spins on the pyrochlore lattice. The conventional cubic unit cell consists of 16 spins and the system size has $N = 3456$ spins. We used the standard Metropolis algorithm where a Monte Carlo step (MCs) is defined as N random single-spin-flip attempts. To improve the quality of the simulations, parallel tempering [7, 8] and over-relaxation [9] were included in the simulations.

The error bars in Fig. 1 (main text) were obtained by using two different cooling procedures during the equilibration of the simulations. For the first "annealed" procedure, the initial configuration is chosen randomly; the system is then gradually cooled down from high temperature (fixed at 10 K) to the temperature of measurement T during 10^6 MCs; it is then equilibrated at the temperature T during 10^6 additional Monte Carlo steps. Since it is starting from high temperature, the annealed procedure tends to favor the phase with higher entropy, i.e. the U(1) manifold, and provides a lower boundary to the transition temperature. For the second "quenched" procedure, the initial configuration is fixed in the SFM phase; the system is then equilibrated at temperature T during 10^6 additional Monte Carlo steps. Since it starts in the ordered SFM phase, the quenched procedure favors the SFM phase and provides an upper boundary to the transition temperature. Following these equilibration procedures, measurements are done every 10 MCs during 10^7 MCs.

For the phase diagram of Fig. 3 b) (main text), the system size was 3456 sites with measurements during 10^6 MCs. For the structure factors of Fig. 3 a) (main text), no parallel tempering was necessary for simulations above the transition temperature. The system size was 128000 sites with measurements during 10^6 MCs.

CLASSICAL LOW-TEMPERATURE EXPANSION

Classical low-temperature expansion is an expansion in small fluctuations around an ordered state of classical spins. It enables calculation of the free energy of a given ordered phase up to leading term in temperature. We have used it to determine the low-temperature dependence of the phase boundary between the SFM and ψ_3 phases, for comparison with MC simulation as indicated by the green line in Fig. 1 of the main text. The method is a standard one, outlined in (e.g.) Ref. [10].

LINEAR SPIN WAVE THEORY

Linear spin wave theory (LSW) is a semi-classical method to study the stability of a classical phase in presence of the quantum zero-point energy. When the phase is a classical ground state, such as the SFM phase in the double-transition region of our paper, the method is rather straightforward. But if the phase is *not* a classical ground state, such as the U(1) manifold in the double-transition region, the inclusion of zero-point energy requires a variation of the LSW theory, as proposed in Ref. [11] and outlined below.

At first, the approach is similar to standard spin wave expansion. We rewrite the spin operators $\vec{S}_i$ in terms of Holstein-Primakoff bosons and perform a $1/S$ expansion around the local spin configuration of the chosen ordered state. At the harmonic level, our Hamiltonian takes the form $\mathcal{H} \approx \mathcal{H}_{\mathsf{LSW}} = \mathcal{H}_{\mathsf{LSW}}^{(0)} + \mathcal{H}_{\mathsf{LSW}}^{(1)} + \mathcal{H}_{\mathsf{LSW}}^{(2)}$. $\mathcal{H}_{\mathsf{LSW}}^{(0)}$ is simply the classical energy of the ordered state around which we are expanding, while $\mathcal{H}_{\mathsf{LSW}}^{(1)}$ and $\mathcal{H}_{\mathsf{LSW}}^{(2)}$ contain only linear and quadratic terms in boson operators, respectively.

If the chosen ordered state is a classical ground state, then $\mathcal{H}_{\mathsf{LSW}}^{(1)}$ must vanish. As for $\mathcal{H}_{\mathsf{LSW}}^{(2)}$, it can be diagonalized by Fourier transform followed by a Bogoliubov transformation which will return real, positive, frequencies and therefore a meaningful excitation spectrum. The semi-classical energy can then be written

$$E_{\mathsf{semi-cl}}^0 = E_{\mathsf{cl}}^0 \left(1 + \frac{1}{S}\right) + \frac{1}{2} \sum_{\vec{k}\lambda} \omega_{\vec{k}\lambda}, \qquad (7)$$

where E_{cl}^0 is the classical ground state energy, $\omega_{\vec{k}\lambda}$ is the spin wave dispersion of band λ at wave-vector $\vec{k}$.

However, if the chosen ordered state is *not* a classical ground state, then $\mathcal{H}_{\mathsf{LSW}}^{(1)}$ may still vanish if the spin configuration we are expanding around is a *saddle point* of the classical energy. As shown in Ref. [2], this is the case for the ψ_2 and ψ_3 configurations. The last remaining point is the diagonalization of $\mathcal{H}_{\mathsf{LSW}}^{(2)}$. Following the approach developed by Coletta *et al.* [11], we add to $\mathcal{H}_{\mathsf{LSW}}^{(2)}$ the positive definite term $V = \delta \sum_i a_i^\dagger a_i$, where the $a_i^\dagger$ and a_i operators are Holstein-Primakoff bosons. This additional term V does not change the classical energy and the parameter δ may be adjusted to the minimum value for which we can obtain a real, positive excitation spectrum. The energy calculated with the inclusion of V is

$$E_{\mathsf{semi-cl}}^\delta = E_{\mathsf{cl}} \left(1 + \frac{1}{S}\right) - N\frac{\delta}{2} + \frac{1}{2} \sum_{\vec{k}\lambda} \omega_{\vec{k}\lambda}^\delta \qquad (8)$$

where E_{cl} is the classical energy of the saddle-point configuration and $\omega_{\vec{k}\lambda}^\delta$ is the spin wave dispersion calculated including the potential V. Since V is a positive definite operator, $E_{\mathsf{semi-cl}}^\delta$ is an upper bound on the semiclassical energy of the saddle-point configuration.
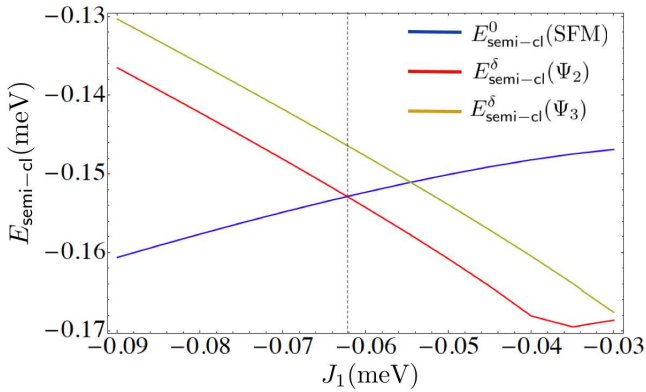
FIG. 1. Semiclassical energy of the SFM states and upper bounds of the ψ_2 and ψ_3 semiclassical energies as a function of J_1 (in meV). The exchange parameters are fixed to $J_2 = -0.22$ meV, $J_3 = -0.29$ meV and $J_4 = 0$. The dashed line is the estimated frontier at $J_1 = -0.062$ meV (see main text).

The SFM semiclassical energy from Eq. (7) (standard approach) and the upper bounds of the ψ_2 and ψ_3 semiclassical energies from Eq. (8) (approach of Ref. [11]) are plotted in Fig. 1. The semiclassical boundary is found to be at $J_1 = -0.062$ meV, as written in Table 1 of the main text.

EXACT DIAGONALIZATION

We consider the properties of the exchange Hamiltonian shown in Eq. (1) of the main text for a single tetrahedron ($N = 4$) and a single cubic unit cell of the pyrochlore lattice ($N = 16$) with periodic boundary conditions. Thanks to the small number of sites the full
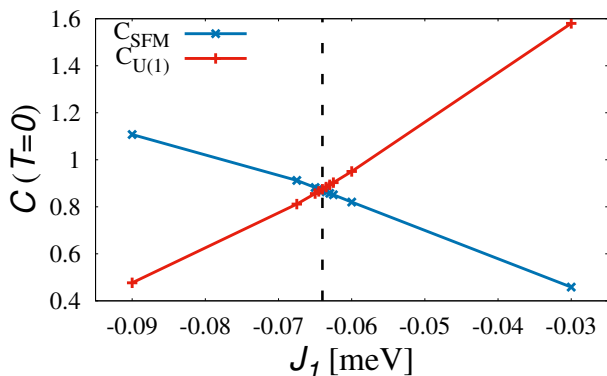

FIG. 2. Correlators $C_{U(1)}$ and C_{SFM} computed via Exact Diagonalization (ED) for $N = 16$ sites at zero temperature as a function of J_1 (in meV). The exchange parameters are fixed to $J_2 = -0.22$ meV, $J_3 = -0.29$ meV and $J_4 = 0$. The dashed line is the estimated frontier at $J_1 \approx -0.064$ meV (see main text).

spectrum is analytically accessible for $N = 4$ and the lowest lying eigenstates can be easily found via standard Lanczos diagonalization for $N = 16$.

As explained in the main text and plotted in Fig. 2, we compare the correlators C of Eq. (5) of the U(1) and SFM ordered phases to determine the boundary between the two phases at zero temperature. This gives the frontier at $J_1 \approx -0.064$ meV, given in Table 1 of the main text.

NUMERICAL LINKED CLUSTER EXPANSION

At finite temperature, we have also performed a numerical linked cluster expansion (NLC) [12, 13], defined as

$$P(\mathcal{L})/N = \sum_{\mathcal{C} \subset \mathcal{L}} L(\mathcal{C})W(\mathcal{C}) \qquad (9)$$

where P is some extensive quantity and N is the number of lattice sites. The sum runs over clusters $\mathcal{C}$ of the lattice, $L(\mathcal{C})$ counts the number of clusters of type $\mathcal{C}$ per site and $W(\mathcal{C})$ is the weight evaluated on the cluster. This weight is computed using inclusion-exclusion rule

$$W(\mathcal{C}) = P(\mathcal{C}) - \sum_{\mathcal{C}' \subset \mathcal{C}} W(\mathcal{C}') \qquad (10)$$

where $P(\mathcal{C})$ is the quantity computed on the cluster $\mathcal{C}$ and the sum runs over proper subclusters of $\mathcal{C}$. There is some freedom in choosing the classes of clusters to sum over in this expansion. We follow the approach of Ref. [14] and use tetrahedra as our building block. A linked cluster with n_T tetrahedra will have at most $3n_T + 1$ sites so we are limited to $n_T \leq 4$ in the expansion. The properties, P, to be computed, are defined on the tetrahedron and so conform well to this expansion.

For convenience, we reproduce in Table I the geometrical clusters used in Ref. [14], with the appropriate embedding constant. These include the 0th order point up to 4th order which includes clusters composed of four tetrahedra. Each cluster has an associated Hamiltonian $H_{\mathcal{C}}$ obtained from the exchange Hamiltonian (Eq. (1) of the main text) which we diagonalize numerically. The largest $n_T = 4$ clusters we consider have 13 sites and thus Hilbert spaces of dimension $2^{13} = 8192$. These remain amenable to full diagonalization and thus we can compute arbitrary thermodynamic quantities at finite temperature.

The series is organized into terms P_n including up to n tetrahedra. Explicitly carrying out the expansion using the embedding constants one has
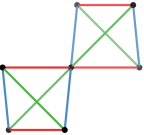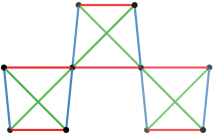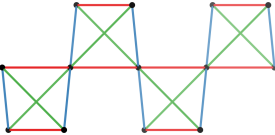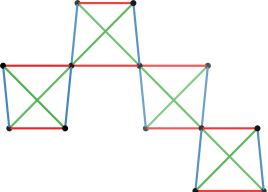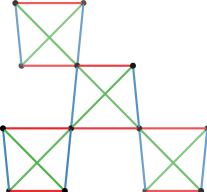
$\mathcal{C}$	$L(\mathcal{C})$		$\mathcal{C}$	$L(\mathcal{C})$
$\mathcal{C}_0$	1	•		
$\mathcal{C}_1$	$\frac{1}{2}$		$\mathcal{C}_2$	1
$\mathcal{C}_3$	3		$\mathcal{C}_{4a}$	3
$\mathcal{C}_{4b}$	6		$\mathcal{C}_{4c}$	2

TABLE I. Clusters used for the NLC expansion. A graphical representation is shown along with the embedding constant $L(\mathcal{C})$.

$$P_0 = +P(\mathcal{C}_0) \tag{11}$$

$$P_1 = -P(\mathcal{C}_0) + \frac{1}{2}P(\mathcal{C}_1) \tag{12}$$

$$P_2 = -\frac{3}{2}P(\mathcal{C}_1) + P(\mathcal{C}_2) \tag{13}$$

$$P_3 = +\frac{3}{2}P(\mathcal{C}_1) - 5P(\mathcal{C}_2) + 3P(\mathcal{C}_3) \tag{14}$$

$$P_4 = -\frac{1}{2}P(\mathcal{C}_1) + 10P(\mathcal{C}_2) - 21P(\mathcal{C}_3)$$
$$+ 3P(\mathcal{C}_{4a}) + 6P(\mathcal{C}_{4b}) + 2P(\mathcal{C}_{4c}) \tag{15}$$

Note that $P(\mathcal{C}_0)$ does not appear directly past first order. Following Ref. [14] the Euler resummation method is used on the final two terms to accelerate convergence. If we define the differences $S_n = P_n - P_{n-1}$ then the Euler approximants are given by

$$E_2 = P_2 \tag{16}$$

$$E_3 = E_2 + \frac{1}{2}S_3 \tag{17}$$

$$E_4 = E_3 + \frac{1}{4}(S_3 + S_4) \tag{18}$$

The difference between 3rd and 4th order of expansion is the uncertainty of our NLC computations.

HIGH TEMPERATURE EXPANSION

The High Temperature Expansions (HTE) are done up to order β^8, as explained in the book of Ref. [15]. The series expansion are then analyzed using Padé approximants, i.e. based on rational functions. We constructed all near-diagonal Padé approximants with 8 or 7 terms in the series, i.e. [4/4], [5/3], [3/5], [6/2], [2/6], [4/3], [3/4], [5/2], [2/5] where [m/n] stand for the powers of the polynomial in the numerator and the denominator. The resulting spread in Padé approximant values represents the error bars of our HTE computations.

Please find attached the coefficients $a_{i=0,..,8}$ of the high-temperature expansion $\sum_i a_i \beta^i$ of the correlators defined in Eq. (5), for different values of J_1 [meV]. The coefficients are correct up to 10 significant digits.

[1] G.-W. Chern, arXiv (2010), arXiv:1008.3038 [cond-mat.str-el].
[2] L. Savary, K. A. Ross, B. D. Gaulin, J. P. C. Ruff, and L. Balents, Phys. Rev. Lett. **109**, 167201 (2012).
[3] M. E. Zhitomirsky, M. V. Gvozdikova, P. C. W. Holdsworth, and R. Moessner, Phys. Rev. Lett. **109**, 077204 (2012).
[4] H. Yan, O. Benton, L. D. C. Jaubert, and N. Shannon, arXiv:1311.3501 (2013).
[5] P. A. McClarty, P. Stasiak, and M. J. P. Gingras, Phys. Rev. B **89**, 024425 (2014).
[6] K. A. Ross, L. Savary, B. D. Gaulin, and L. Balents, Physical Review X **1**, 021002 (2011).
[7] R. H. Swendsen and J.-S. Wang, Phys. Rev. Lett. **57**, 2607 (1986).
[8] C. J. Geyer, Computing Science and Statistics: Proceedings of the 23rd Symposium on the Interface , p. 156 (1991).
[9] M. Creutz, Physical Review D **36**, 515 (1987).
[10] N. Shannon, K. Penc, and Y. Motome,

Phys. Rev. B **81**, 184409 (2010).

[11] T. Coletta, M. E. Zhitomirsky, and F. Mila, Phys. Rev. B **87**, 060407 (2013).

[12] M. Rigol, T. Bryant, and R. R. P. Singh, Physical Review E **75**, 061118 (2007).

[13] B. Tang, E. Khatami, and M. Rigol, Computer Physics Communications **184**, 557 (2013).

[14] R. Applegate, N. R. Hayre, R. R. P. Singh, T. Lin, A. G. R. Day, and M. J. P. Gingras, Phys. Rev. Lett. **109**, 097205 (2012).

[15] J. Oitmaa, C. Hamer, and W. Zheng, *Series Expansion Methods for Strongly Interacting Lattice Models* (Cambridge University Press, Cambridge, UK, 2006).